ACS OMEGA

http://pubs.acs.org/journal/acsodf

Article

Effect of Annealing on Graphene/PVDF Nanocomposites

Victor K. Samoei, Surendra Maharjan, Keiichiro Sano, and Ahalapitiya H. Jayatissa*

Cite This: *ACS Omega* 2023, 8, 13876−13883

Read Online

ACCESS | Metrics & More | Article Recommendations

ABSTRACT: In this study, the process for tuning the electrical properties of graphene/polyvinylidene fluoride (Gr/PVDF) nanocomposite films by a thermal annealing process is explored. The surface morphology and microstructure of the nanocomposite were characterized. The effect of temperature on the electrical conductivity was investigated by heating and cooling the sample from the room temperature up to 150 °C. The effect of annealing on the electrical conductivity was recorded as a function of annealing temperature. A Hall effect measurement was conducted as a function of annealing temperatures to obtain Hall voltage (V_H), carrier mobility (μ_H), carrier concentration (n_H), Hall coefficient (R_H), resistivity, and carrier conductivity type (n or p). It was found that the films annealed at 150 °C exhibited the best electrical conductivity of Gr/PVDF films. This study may provide an insight into the development and utilization of Gr/PVDF films in future electronics and the potential applications in various sectors such as aerospace, automotive, and biomedical industries.

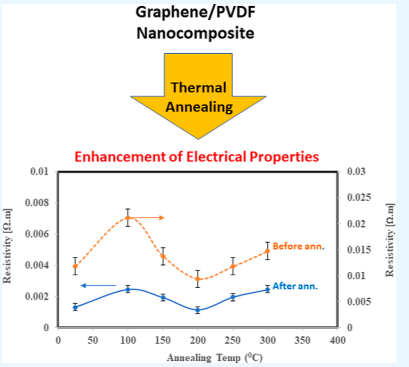

1. INTRODUCTION

Graphene is a two-dimensional crystal structure of sp^2-hybridized carbon atom,[1] bound in a hexagonal honeycomb lattice structure. The sp^2-hybridized bond in graphene comprises three σ-bonds and one π-bond, with a molecular bond length of 0.142 nm and an interplanar spacing of 0.335 nm.[2] In-plane $\sigma_{C\text{-}C}$ bond is the strongest bond that holds the carbon atoms tightly together and out-of-plane π-bond, which creates weak van der Waals interactions between the graphene layers of graphene/polymer. This imparts the delocalization of the π-cloud, leading to the conduction of electrons. Besides, the other two reasons for superior conductivity in graphene are zero band gap and relativistic velocity of electrons and holes. Because of zero band gaps, graphene is also known as a semimetal. Graphene layers are stacked together to form graphite, and the weak van der Waals forces between the layers can be overcome during the exfoliation of graphene by different techniques. Since the discovery of graphene in 2004,[3,4] extensive research has been performed to take advantage of its excellent physical, chemical, electrical, and mechanical properties such as very high specific surface area (2300 m^2/g), electrical conductivity (6×10^3 S/cm), light transmittance (97.7% for single layer), thermal conductivity (5000 W/mK at the room temperature), and tensile strength and shear modulus (130 GPa and 1.0 TPa).[5−8]

Graphene nanoparticles were selected for this investigation owing to their stability, high conductivity, easily availability, and low cost.[9] Recently, a new class of materials called MXene has been identified as a filler material in composite materials owing to important MXane's properties such as tunability of properties choosing the metal component (M). MXene nanosheet-based hydrogel composites have been successfully developed to fabricate triboelectric nanogenerators.[10] However, this material also has some challenges in application viewpoints such as the poor dispersibility of MXene nanosheets in the composites and instability of MXene in the presence of water vapor.[11] Another candidate for nanocomposite fillers is the carbon nanotubes, which have extremely high production cost and relatively low conductivity.[12,13] For example, multiwalled carbon nanotube composites have been successfully used for the applications in energy harvesting and motion sensor applications.[13] Also, polyvinylidene fluoride (PVDF) is an electroactive polymer, and it can be used in many stretchable devices such as pressure sensors, acoustic devices, and accelerometers.[14]

The graphene synthesis process is quite diverse, mainly based upon a top-down or bottom-up approach.[15] The top-down approach is more straightforward because of easily accessible raw materials and easy processing conditions.[16] Single-layer graphite, known as graphene, has attracted considerable scientific interest in recent years due to its outstanding mechanical, thermal, and electrical properties as well as large-surface area. Thus, graphene is an ideal candidate as a nano-filler for improving the mechanical, electrical, and thermal properties of polymers. The most of research activities

Received: January 14, 2023
Accepted: March 20, 2023
Published: April 5, 2023

in this field focused on graphene oxide (GO) or reduced GO (RGO) prior to its dispersion into the polymer matrix. Graphene-based conductive nanocomposites have been investigated using poly(methyl methacrylate) and polypyrrole as matrix materials for sensor applications.[17,18] These nanocomposites produce multilayer platelets rather than single-layer sheets. Tang et al. first demonstrated that a solution cast film can be thermally reduced without employing hazardous reducing agents such as dimethylhydrazine.[19] An isolated single layer of RGO enhances the thermal and electrical properties at very low percolation values. However, no comprehensive study of piezoelectric enhancement of this composite film has been reported.[20,21]

The PVDF is a semicrystalline polymer with several crystal phases identified as α, β, δ, and γ, produced by the polymerization of vinylidene difluoride. The β-phase of PVDF, which is responsible for unique pyroelectric and piezoelectric properties, provides good processability to prepare flat sheets, hollow fiber, or tubular membranes.[21] It also has a high dielectric constant and resistance to chemicals.[20,21] It is commonly used in semiconductor, chemical, medical, defense aviation, aerospace, and energy storage applications. Generators based on piezoelectricity have become the most widely used devices in various applications due to their high sensitivity, stability, fast response, and parallel-reading detections of spatial pressure distributions.

PVDF is soluble in some common solvents such as *N*, *N*-dimethylacetamide, dimethylformamide (DMF), and *N*-methyl-2-pyrrolidone.[22] The dielectric permittivity of PVDF composites remains low, even when a high concentration of the ceramic filler is used. The weak interfacial interactions and pores in composites might be responsible for low dielectric permittivity of the composites.[23−25] Moreover, the use of ceramic fillers deteriorates the flexibility of the polymer matrix due to high concentration of rigid ceramic particles. The fluorine atoms of PVDF possess a high affinity with carbon atoms; hence, it is also suitable as a binder for graphene. Its binding capability has been utilized in carbon electrodes in supercapacitors and other electrochemical applications too.[26−28] Table 1 gives some important properties of graphene and PVDF materials relevant to this investigation.

Table 1. Physical, Thermal, and Electrical Properties of Graphite and PVDF[29−32]

property	graphene	PVDF
density	2.25 g/cm^3	1.74 g/cm^3
melting point	3650 °C	165 °C
electrical resistivity	10^{-5}−10^{-6} Ω cm	2 × 10^{14} Ω cm
thermal conductivity	1800−5400 W/m K	0.13−0.19 W/m K
dielectric constant (at 23°C)	6−8 (6.9 at 0.22 nm thickness)	6−8
glass-transition temp	5226.85 °C	−40.0 °C
electron mobility	>15,000 (cm^{2}V^{-1} s^{-1})	-

The present work aims at the investigation of the effect of thermal annealing on the electrical properties of graphene/polyvinylidene fluoride (Gr/PVDF) nanocomposites. This composite was used to fabricate flexible piezoresistive pressure sensors with excellent sensitivity.[14,33] However, we did not optimize the electrical properties in the development of the sensor. In this investigation, the post-annealing process was conducted at different temperatures in the range of 100−300 °C. It was found that the electrical conductivity of the composite was improved by annealing up to 150 °C and reaching a saturated level. This composite is a complicated system because the electromechanical properties of PVDF can be substantially changed in this temperature region. In addition, cross-linking and intercalation of the polymer matrix in graphene layers can influence the electrical properties. We believe that this investigation will help better understand the electrical properties of this composite and further explore its applications as a conductor, sensing material, and piezoresistive material.

2. EXPERIMENTAL SECTION

2.1. Preparation. In order to obtain graphene, graphite particles (99.99%) were mixed with DMF as a solvent in the ratio of 0.1 g:4.0 mL. The large particles of graphite were broken down by a milling process before mixing with DMF. After mixing with DMF, the solution was sonicated four times, each for 10 min, keeping an interval of 10 min to prevent aggregation of graphite particles by temperature. After the sonication process was completed, the mixture was kept for 12 h at the static conditions and room temperature. The heavy graphite particles are sedimented in the bottom of the container, and light small particles are suspended in the upper portion of the container. The upper portion was carefully collected using a pipet (by experience) to get the graphene solution. The graphene particles extracted in this method were in 4−5 layers and density (∼1.0 μg/mL) as estimated in our experiments. The PVDF powder (Alfa Aesar, 99.99%), was dissolved in DMF in the ratio of 0.05 g:2.0 mL. The PVDF/DMF solution was stirred and placed in a sonicator for 20 min to ensure that the PVDF powder was completely dissolved. The graphene and PVDF solutions were mixed in a beaker and further sonicated for 2 times (20 min each with 10 min gap) with the same procedure to achieve a homogeneous mixture. The homogeneous Gr/PVDF solution was kept settling for 12 h at room temperature before coating on a glass substrate. The solution was kept at room temperature for 12 h before testing to ensure that the DMF solvent was evaporated. The flowchart preparation is shown in Figure 1. The thickness of the prepared samples was 8.0 μm. The volume content of PVDF in the composite can be determined by the following equation, where m_G and m_P represent the mass of graphite and PVDF, respectively; ρ_G and ρ_P are the density of graphite and PVDF, respectively.[33]

$$\text{Ø}_{vol} = \frac{m_p/\rho_p}{m_p/\rho_p + m_G/\rho_G} \times 100 \quad (1)$$

%

The estimated Ø_{vol} for PVDF in Gr/PVDF was about 97.5%. This estimation indicated that the volume content of graphene in Gr/PVDF is about ∼2.5%, which is very small compared with PVDF. However, the change in electrical conductivity was very large. That is one of the reasons for choosing PVDF as the polymer matric in this investigation.

3. RESULTS AND DISCUSSION

3.1. Material Characterization. *3.1.1. Crystallinity and Morphology.* The XRD measurements were used to investigate the crystalline structures of graphene and PVDF composites. Figure 2 shows the XRD spectrum of Gr/PVDF

https://doi.org/10.1021/acsomega.3c00283
ACS Omega 2023, 8, 13876−13883

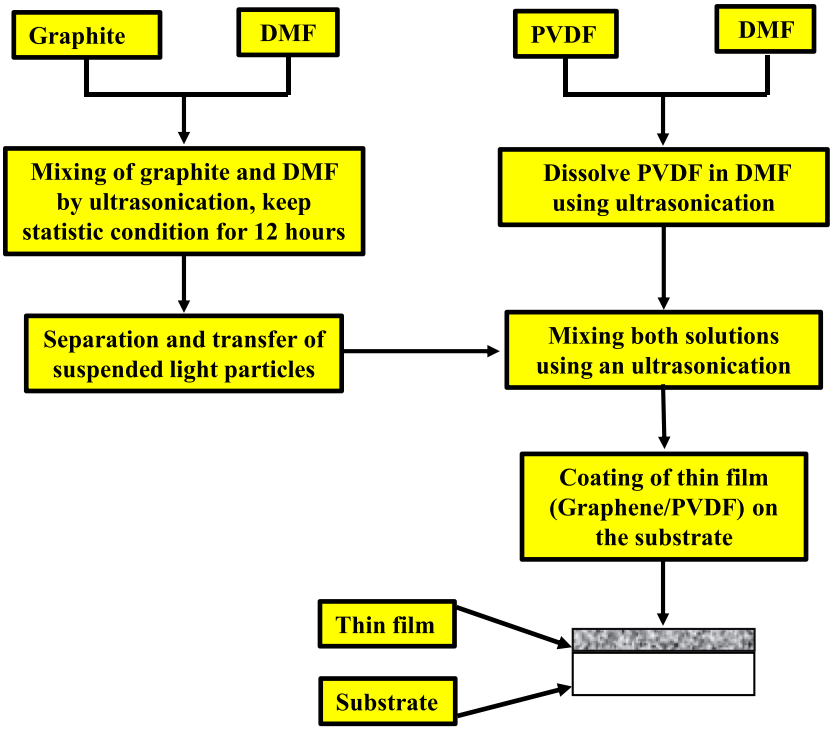

Figure 1. Schematic of the preparation of Gr/PVDF composite films.

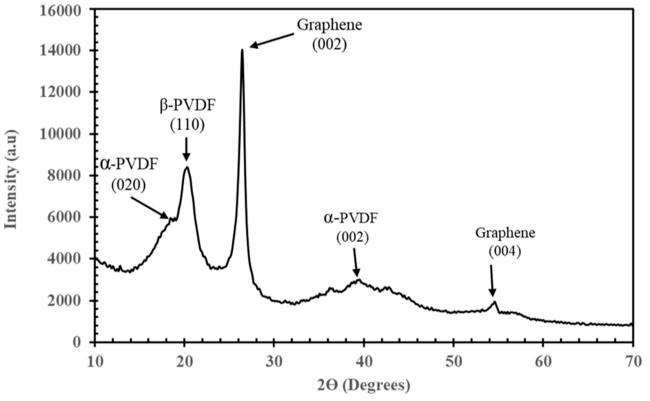

Figure 2. XRD patterns of the Gr/PVDF composite.

nanocomposites for 2θ angle between 10 and 70°. The XRD peaks of graphene and PVDF confirm the presence of these constituents in the nanocomposite.[33,34] The XRD pattern exhibits sharp diffraction peaks corresponding to the 2θ angles of 18.88° [020], 20.48° [110], and 39.64° [020] crystallographic planes of PVDF. The dipole moment of PVDF is primarily responsible for producing the β-phase of PVDF at 20.48°. The characteristic diffraction peaks of the film positioned at approximately 26.42 and 54.56° corresponding to the reflection of crystal planes [002] and [004] of graphene, respectively. Broader peaks indicated that both graphene and PVDF crystallites are very small. The SEM image collected for graphene particles indicated that they are in 3−6 layers. The purpose of our graphene is to enhance the conductivity, and we believe that this size range of graphene is an ideal candidate for electrical conductivity applications because the further reduction of graphene (1−2 layers) produces more semiconducting materials.[33]

Figure 3 shows the SEM images of composites films before annealing and after annealing at 100 and 300 °C. Uniformity of the as-fabricated and annealed films can be compared with the SEM images. The surface roughness of films was drastically reduced in the annealing process. The optical images of Gr/PVDF annealed at different temperatures were captured using an optical microscope at a magnification of 400×, as shown in Figure 4. The images have no cracks and no aggregation of graphene or PVDF, depicting the homogeneous mixing of graphene and PVDF in the composites.

3.1.2. Raman Spectroscopy. Figure 5 shows the Raman spectra recorded for the Gr/PVDF nanocomposites with different annealing temperatures obtained from 400 to 3000 cm $^{-1}$. The Raman spectroscopy provides more information

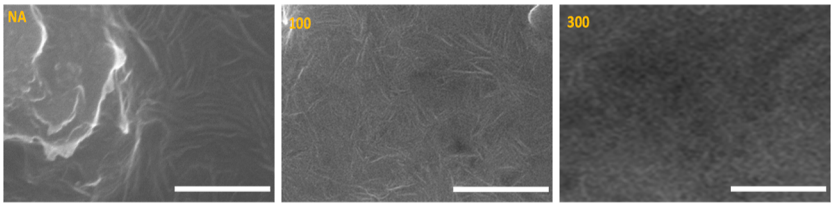

Figure 3. SEM images of Gr/PVDF nanocomposites. Scale bar indicates 500 nm (from left to right: not annealed sample, 100 °C annealed sample, and 300 °C annealed sample).

https://doi.org/10.1021/acsomega.3c00283
ACS Omega 2023, 8, 13876−13883

Figure 4. Optical images of nanocomposites for different annealed temperatures at the magnification of 400× (from left to right: not annealed sample, 100 °C annealed sample, and 300 °C annealed sample).

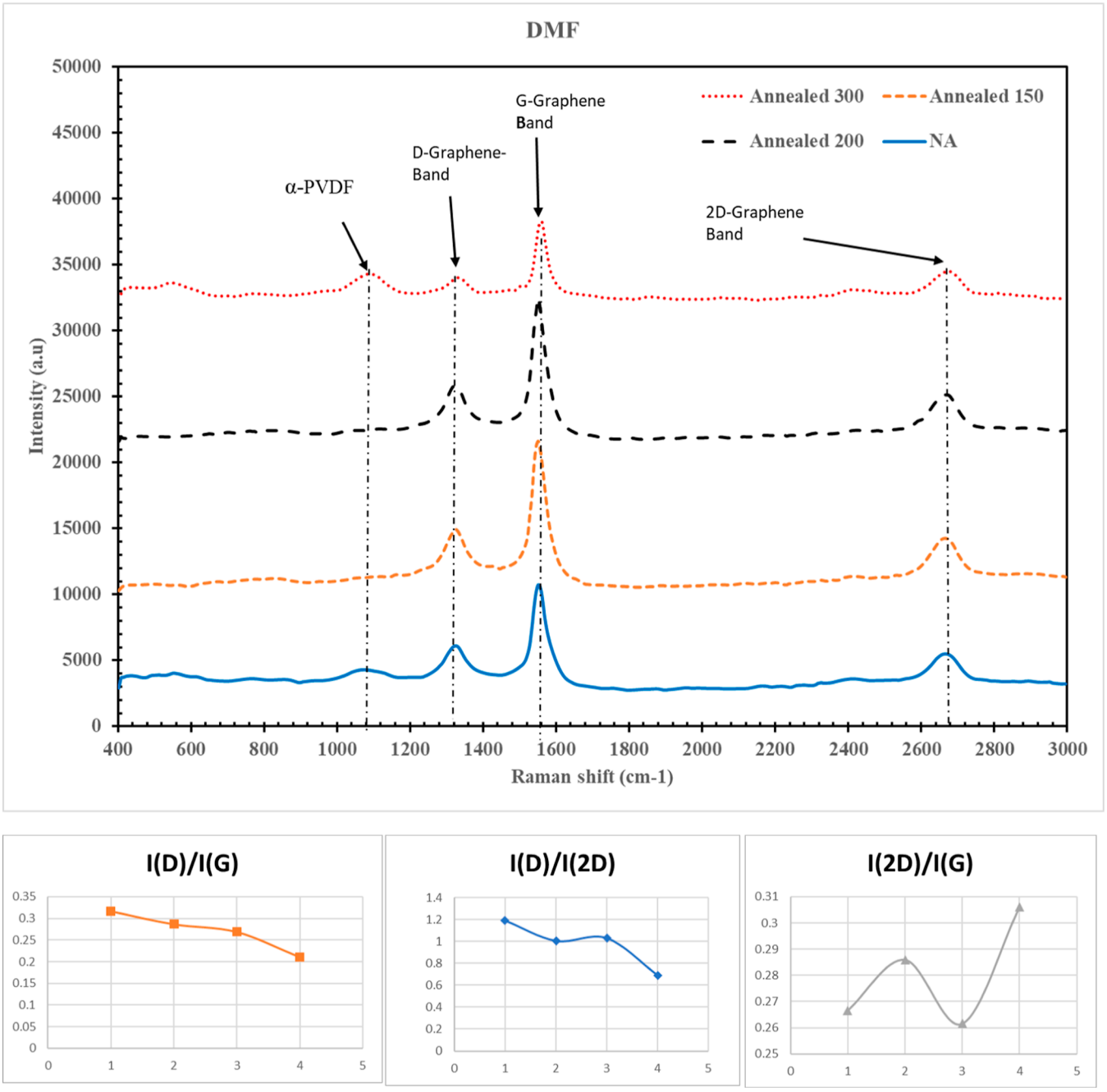

Figure 5. Raman spectra of the Gr/PVDF nanocomposites. Upper figure gives the spectra of annealed films at 150, 200, and 300 °C with unannealed films. Lower three figures (from left to right) indicate the ratios of intensity of D-band/G-band, D-band/2D-band, and 2D-band/G-band as a function of annealing condition. For lower three figures, the *X*-axis indicates: 1-unannealed; 2−150 °C annealed, 3−200 °C annealed, and 4−300 °C annealed samples.

https://doi.org/10.1021/acsomega.3c00283
ACS Omega 2023, 8, 13876−13883

about the conjugated structure and the chained skeleton of polymers. It also yields bands of lower wavenumbers as readily as bands of higher wavenumbers.[35] There are four peaks at 1083, 1341, 1562, and 2681 cm^{-1}. The nanocomposite Raman spectra indicated the formation of the α phase of PVDF with one peak at 1083 cm^{-1}, the peak appeared predominantly for not annealed and 300 °C annealed samples. Samples annealed at 150 and 200 °C did not show any dominant peak for PVDF. Three dominant peaks for graphene appeared at 1341, 1562, and 2681 cm^{-1} attributed to the D, G, and 2D bands, respectively. The peak intensity around 2680 cm $^{-1}$(2D peak) was about twice that of the G peak. The intensity ratio of I_G/I_{2D} indicated the presence of multilayer graphene present in the nanocomposite, and the I_G/I_D was about 0.25 for all films, indicating that the film had few defects. Also, the lowest value of I_G/I_D was given for the films annealed at 300 °C (Figure 5b). It was seen that the quality of graphene was improved by reducing the defects of graphene during the annealing process.[36,37]

3.2. Effect of Annealing on Electrical Conductivity. The resistance of the Gr/PVDF thin films was measured before and after the annealing process, as given in Figure 6. It can be

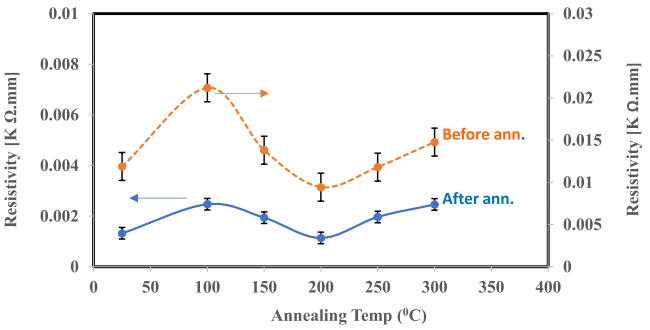

Figure 6. Resistivity of Gr/PVDF as a function of temperature before annealing and after annealing. Since these samples represent different samples before and after annealing, in the comparison, the resistivities of each sample before annealing and after annealing are shown.

observed from the graphs that resistance drops after annealing. The conductivity was calculated using the following relationships ($R = \rho l/A$), where ρ is the resistivity, R is the resistance, l is the length, $\sigma = 1/\rho$ is the conductivity, and A is the cross-sectional area (thickness × width of electrode in contact). The change of conductivity ($\sigma_{annealed} - \sigma_{unannealed}$) and percent change in conductivity [$(\sigma_{annealed} - \sigma_{unannealed})/\sigma_{unannealed}) \times 100\%$] were plotted, and results are given in Figure 7. The improvement in conductivity can be attributed to the reduction of graphene defects and enhanced cross-links in the PVDF matrix in the annealing process. The contact resistance at the interface of graphene/polymer is improved by annealing because graphene forms an interconnected conductive pre-network.[38] Temperature also plays an important role in crystal structure formation of PVDF films; heat increases the degree of crystallinity in the beta phase of PVDF. These combined effects can be the primary reasons for outstanding electrical characteristics.[39] Temperature in the range of 70−170 °C is the favorable annealing process for PVDF thin films with high dielectric constant, low tangent loss, and high resistivity.[40]

3.3. Temperature Dependence on Electrical Conductivity. The relation between resistance and temperature in

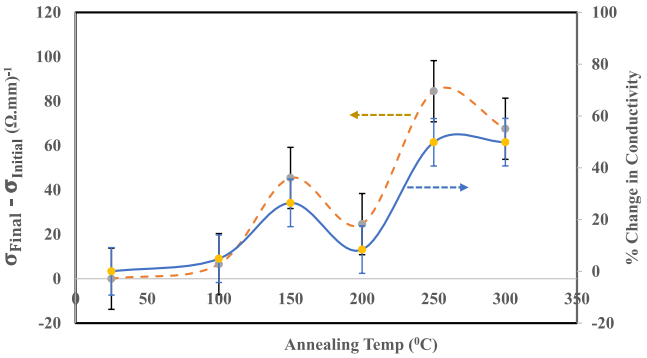

Figure 7. Change of conductivity in Gr/PVDF films with different annealing temperatures (right side gives ($\sigma_{annealed} - \sigma_{unannealed}$)/$\sigma_{unannealed}$) × 100%, and left side gives ($\sigma_{annealed} - \sigma_{unannealed}$).

the insulator and semiconductor material is given by the Arrhenius behavior given below

$$R = R_0 \times \exp\left(\frac{E_a}{K_b \times T}\right) \quad (2)$$

Taking logs and rearranging, we get

$$\ln R = \left(\frac{E_a}{K_b}\right) \times \frac{1}{T} + \ln R_0 \quad (3)$$

Here, K_b is the Boltzmann constants, and E_a gives the thermal activation energy of electrical conductivity of the sample. The composites were coated on a glass substrate and annealed at different temperatures to measure the electrical resistance. Two gold terminals were connected to the annealed and non-annealed samples. The samples were heated from room temperature to 150 °C using a resistance heater under vacuum conditions, and a thermocouple was used to measure the surface temperature of composites. The resistance was recorded after every increment of 5 °C through a multimeter (Keithley 2020). It was then cooled gradually from 150 °C to room temperature, and the resistance was recorded. Figure 8 is plotted for different samples using eq 3. It is observed from the graph that the electrical conductivity rose with an increase in temperature. This can be depicted as the semiconductor nature of the nanocomposite.[33,41] Also, all lines of Arrhenius plots are in parallel, indicating that the E_a (0.02 eV/K) did not

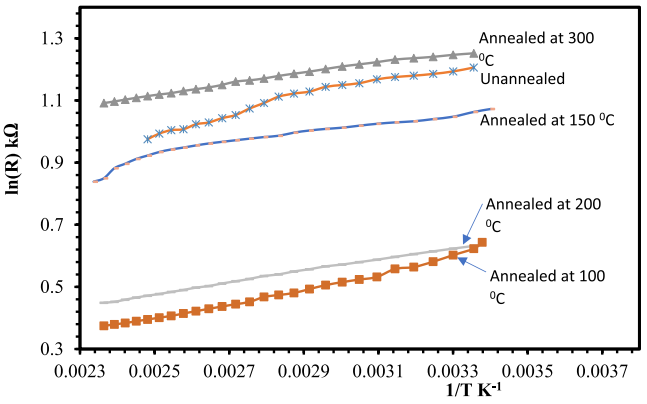

Figure 8. Arrhenius plots of resistance (R) versus reciprocal of temperature ($1/K$) for Gr/PVDF composites annealed at different temperatures.

https://doi.org/10.1021/acsomega.3c00283
ACS Omega 2023, 8, 13876−13883

significantly change due to the annealing process. Also, such a low E_a value clearly indicates that the electrical conductivity of composites is predominantly controlled by the graphene.

3.4. Hall Effect. The Hall effect measurement is useful for characterizing semiconductor material in terms of Hall voltage (V_H), carrier mobility (μ_H), carrier concentration (n_H), Hall coefficient (R_H), resistivity, and carrier conductivity type (n or p). Hall voltage is the one measured, and other parameters are the derivatives of Hall voltage.[42]

Figure 9 shows the carrier mobility and carrier concentration of annealed and unannealed Gr/PVDF nanocomposites. The

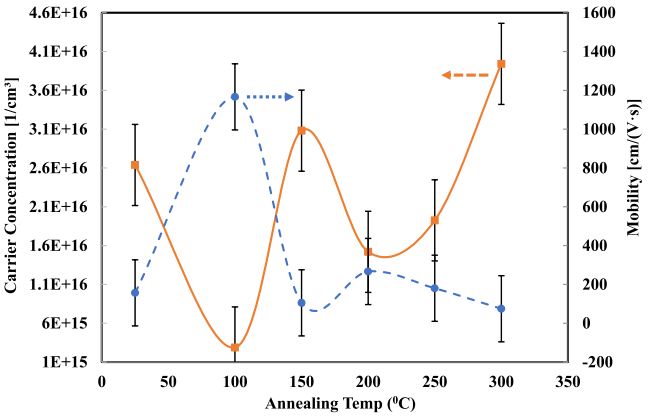

Figure 9. Carrier concentration and Hall mobility of Gr/PVDF with annealing temperature.

mobility of charge carriers was found to be higher at 100 °C, and some changes could also be seen at 200 °C. However, at other annealed temperatures, the effect of annealing was not clearly visible in terms of Hall mobility. The carrier concentration was the highest at 300 °C, and it can be attributed to the good bonding of carbon between graphene and fluorine from PVDF, hence releasing the charge carriers. On the other hand, even with higher carrier concentrations at 300 °C, Hall mobility was low. The nanocomposite changed from p-type to n-type when annealed at a temperature above 100 °C. We believe that such changes are attributed to the oxygen adsorption/desorption and the diffusion mechanism that depends on temperature. At room temperature, oxygen absorbed in graphene exhibits p-type behavior but after annealing in the range of 100−250 °C, the oxygen is released from the graphene.[43] It should be noted that the increase in the majority carrier concentration leads to a strong decrease in mobility, which indicates ionized impurity scattering as a major factor limiting mobility in this composite, which is commonly observed in references 44. 45,

In addition to the electrical property enhancement, the effect of annealing on the mechanical properties of Gr/PVDF nanocomposites should be investigated. Investigations are undertaken to understand the mechanical properties of annealed Gr/PVDF nanocomposites. It should be noted that annealing improves the adhesion and stability of Gr/PVDF nanocomposites at cyclic mechanical vibrations. More quantitative and qualitative measurements will be reported in the future.

4. CONCLUSIONS

In summary, Gr/PVDF films with uniform thickness and good electrical conductivity were successfully prepared by a solution-phase mixing technique. A series of prepared Gr/PVDF nanocomposite films were annealed for 2 h at different temperatures (100−300 °C) to study the electrical properties as a function of annealing temperature. The effect of annealing on the composite was investigated by recording the changes before and after annealing, and it was found that the annealing improved the electrical conductivity of the nanocomposite. We concluded that the interfacial configuration between graphene and PVDF was improved in the annealing process. The improved interconnect has an important influence on electrical conduction and thermal transportation at the interface of graphene and PVDF. The graphene-network architecture and graphene alignment in the nanocomposite are important to take full advantage of the 2D feature of graphene for various applications.

AUTHOR INFORMATION

Corresponding Author

Ahalapitiya H. Jayatissa − *Nanotechnology and MEMS Laboratory, Department of Mechanical, Industrial, and Manufacturing Engineering (MIME), The University of Toledo, Toledo, Ohio 43606, United States;* orcid.org/0000-0003-2478-2994; Email: ahalapitiya.jayatissa@utoledo.edu

Authors

Victor K. Samoei − *Nanotechnology and MEMS Laboratory, Department of Mechanical, Industrial, and Manufacturing Engineering (MIME), The University of Toledo, Toledo, Ohio 43606, United States*

Surendra Maharjan − *Nanotechnology and MEMS Laboratory, Department of Mechanical, Industrial, and Manufacturing Engineering (MIME), The University of Toledo, Toledo, Ohio 43606, United States*

Keiichiro Sano − *Materials & Surface Engineering Research Institute, Kanto Gakuin University, Odawara-shi, Kanagawa 250-0042, Japan*

Complete contact information is available at: https://pubs.acs.org/10.1021/acsomega.3c00283

Author Contributions

All authors have given approval to the final version of the manuscript.

Notes

The authors declare no competing financial interest.

ACKNOWLEDGMENTS

S.M. and V.K.S. would like to thank the University of Toledo (UT) for providing stipends for this research through graduate assistantships (GA). Also, the authors thank Dr. Yanfa Yan and Dr. Zhaoning Song of the Department of Physics and Astronomy of UT for permission to use their Hall Effect measurement system. The authors would also like to thank Dr. A. C. Jayasuriya and A. Bharadwaz for their support in Raman spectroscopy. One of the authors (K.S.) would like to acknowledge partial support provided by the Engineering Research Institute of Kanto Gakuin University for this research.

REFERENCES

(1) Geim, A. K.; Novoselov, K. S. The rise of graphene. *Nat. Mater.* **2007**, *6*, 183−191.

https://doi.org/10.1021/acsomega.3c00283
ACS Omega 2023, 8, 13876−13883

(2) Chung, D. D. L. Review Graphite. *J. Mater. Sci.* **2002**, *37*, 1475−1489.
(3) Novoselov, K. S.; Jiang, D.; Schedin, F.; Booth, T. J.; Khotkevich, V. V.; Morozov, S. V.; Geim, A. K. Two-dimensional atomic crystals. *Two-dimensional atomic crystals. Proc. Natl. Acad. Sci.* **2005**, *102*, 10451−10453.
(4) Meyer, J. C.; Geim, A. K.; Katsnelson, M. I.; Novoselov, K. S.; Booth, T. J.; Roth, S. The structure of suspended graphene sheets. *Nature* **2007**, *446*, 60−63.
(5) Bolotin, K. I.; Sikes, K. J.; Jiang, Z.; Klima, M.; Fudenberg, G.; Hone, J.; Kim, P.; Stormer, H. Ultrahigh electron mobility in suspended graphene. *Solid state communications* **2008**, *146*, 351−355.
(6) Kim, K. S.; Zhao, Y.; Jang, H.; Lee, S. Y.; Kim, J. M.; Kim, K. S.; Ahn, J. H.; Kim, P.; Choi, J. Y.; Hong, B. H. Large-scale pattern growth of graphene films for stretchable transparent electrodes. *Nature* **2009**, *457*, 706−710.
(7) Balandin, A. A.; Ghosh, S.; Bao, W.; Calizo, I.; Teweldebrhan, D.; Miao, F.; Lau, C. N. Superior thermal conductivity of single-layer graphene. *Nano letters* **2008**, *8*, 902−907.
(8) Nair, R. R.; Blake, P.; Grigorenko, A. N.; Novoselov, K. S.; Booth, T. J.; Stauber, T.; Peres, N. M. R.; Geim, A. K. Fine structure constant defines visual transparency of graphene. *Science* **2008**, *320*, 1308.
(9) Itapu, B.; Jayatissa, A. H. A Review in Graphene/Polymer Composites. *Chem. Sci. Int. J.* **2018**, *23*, 1−16.
(10) Zhang, H.; Zhang, D.; Wang, Z.; Xi, G.; Mao, R.; Ma, Y.; Wang, D.; Tang, M.; Xu, Z.; Luan, H. Ultrastretchable, Self-Healing Conductive Hydrogel-Based Triboelectric Nanogenerators for Human−Computer Interaction. *ACS Appl. Mater. Interfaces* **2023**, *15*, 5128−5138.
(11) Wang, Q.; Pan, X.; Wang, X.; Cao, S.; Chen, l.; Ma, X.; Huang, L.; Ni, Y. Fabrication strategies and application fields of novel 2D Ti3C2Tx (MXene) composite hydrogels: A mini review. *Ceram. Int.* **2021**, *47*, 4398−4403.
(12) Prolongo, S. G.; Moriche, R.; Jiménez-Suárez, A.; Sánchez, M.; Ureña, A. Advantages and disadvantages of the addition of graphene nanoplatelets to epoxy resins. *Eur. Polym. J.* **2014**, *61*, 206−214.
(13) Zhang, H.; Zhang, D. Z.; Wang, D. Y.; Xu, Z. Y.; Yang, Y.; Zhang, B. Flexible single-electrode triboelectric nanogenerator with MWCNT/PDMS composite film for environmental energy harvesting and human motion monitoring. *Rare Metals* **2022**, *41*, 3117−3128.
(14) Maharjan, S.; Samoei, V. K.; Jayatissa, A. H. Graphene/PVDF Nanocomposite-Based Accelerometer for Detection of Low Vibrations. *Materials* **2023**, *16*, 1586−1566.
(15) Pusty, M.; Shirage, P. M. Insights and perspectives on graphene-PVDF based nanocomposite materials for harvesting mechanical energy. *J. Alloys Compd.* **2022**, *904*, 164060.
(16) Kumar, N.; Salehiyan, R.; Chauke, V.; Joseph Botlhoko, O.; Setshedi, K.; Scriba, M.; Masukume, M.; Sinha Ray, S. Top-down synthesis of graphene: A comprehensive review. *FlatChem* **2021**, *27*, 100224.
(17) Wang, W.; Jayatissa, A. H. Comparison study of graphene based conductive nanocomposites using poly(methyl methacrylate) and polypyrrole as matrix materials. *J. Mater. Sci. Mater. Electron.* **2015**, *26*, 7780−7783.
(18) Wang, W.; Jayatissa, A. H. Computational and experimental study of electrical conductivity of graphene/poly(methyl methacrylate) nanocomposite using Monte Carlo method and percolation theory. *Synth. Met.* **2015**, *204*, 141−147.
(19) Tang, H.; Ehlert, G. J.; Lin, Y.; Sodano, H. A. Highly efficient synthesis of graphene nanocomposites. *Nano letters* **2012**, *12*, 84−90.
(20) Ansari, S.; Giannelis, E. P. Functionalized graphene sheet poly (vinylidene fluoride) conductive nanocomposites. *Journal of Polymer Science Part B: Polymer Physics* **2009**, *47*, 888−897.
(21) Zhu, Y.; Murali, S.; Cai, W.; Li, X.; Suk, J. W.; Potts, J. R.; Ruoff, R. S. Graphene and graphene oxide: synthesis, properties, and applications. *Advanced materials* **2010**, *22*, 3906−3924.
(22) Zhu, C.; Du, D.; Lin, Y. Graphene and graphene-like 2D materials for optical biosensing and bioimaging: A review. *2D Materials* **2015**, *2*, 032004.
(23) Yeow, M. L.; Liu, Y. T.; Li, K. Isothermal phase diagrams and phase-inversion behavior of poly (vinylidene fluoride)/solvents/additives/water systems. *J. Appl. Polym. Sci.* **2003**, *90*, 2150−2155.
(24) Dang, Z. M.; Zhou, T.; Yao, S. H.; Yuan, J. K.; Zha, J. W.; Song, H. T.; Li, J. Y.; Chen, Q.; Yang, W. T.; Bai, J. Advanced calcium copper titanate/polyimide functional hybrid films with high dielectric permittivity. *Adv. Mater.* **2009**, *21*, 2077−2082.
(25) Luo, B.; Wang, X.; Wang, Y.; Li, L. Fabrication, characterization, properties and theoretical analysis of ceramic/PVDF composite flexible films with high dielectric constant and low dielectric loss. *J. Mater. Chem.* **2014**, *2*, 510−519.
(26) Frackowiak, E.; Beguin, F. Carbon materials for the electrochemical storage of energy in capacitors. *Carbon* **2001**, *39*, 937−950.
(27) Diederich, L.; Barborini, E.; Piseri, P.; Podesta, A.; Milani, P.; Schneuwly, A.; Gallay, R. Supercapacitors based on nanostructured carbon electrodes grown by cluster-beam deposition. *Applied physics letters* **1999**, *75*, 2662−2664.
(28) Ataur Rahman, M.; Chung, G. S. Synthesis of PVDF-graphene nanocomposites and their properties. *J. Alloys Compd.* **2013**, *581*, 724−730.
(29) Lee, S. K.; Kim, H.; Shim, B. S. Graphene: an emerging material for biological tissue engineering. *Carbon letters* **2013**, *14*, 63−75.
(30) Riosbaas, M. T.; Loh, K. J.; O'Bryan, G.; Loyola, B. R.. Sensors and Smart Structures Technologies for Civil Mechanical, and Aerospace Systems, *In situ phase change characterization of PVDF thin films using Raman spectroscopy*, 2014; Vol. *9061*, pp 235−245.
(31) Somphonsane, R.; Ramamoorthy, H.; He, G.; Nathawat, J.; Kwan, C. P.; Arabchigavkani, N.; Lee, Y. H.; Fransson, J. P.; Bird, J. P. Evaluating the sources of graphene's resistivity using differential conductance. *Sci. Rep.* **2017**, *7*, 10317−10411.
(32) Ravinder, R.; Kumar, R.; Agarwal, M.; Krishnan, N. M. A. Evidence of a two-dimensional glass transition in graphene: Insights from molecular simulations. *Sci. Rep.* **2019**, *9*, 4517−4519.
(33) Maharjan, S.; Samoei, V. K.; Amili, O.; Sano, K.; Honma, H.; Jayatissa, A. H. Design and fabrication of a graphene/polyvinylidene fluoride nanocomposite-based airflow sensor. *ACS omega* **2022**, *7*, 7981−7988.
(34) Grannan, D. M.; Garland, J. C.; Tanner, D. B. Critical behavior of the dielectric constant of a random composite near the percolation threshold. *Phys. Rev. Lett.* **1981**, *46*, 375−378.
(35) Wood, S.; Hollis, J. R.; Kim, J. S. Raman spectroscopy as an advanced structural nanoprobe for conjugated molecular semiconductors. *J. Physics D: Appl. Phys.* **2017**, *50*, 073001.
(36) Pramod, K.; Gangineni, R. B. Influence of solvent evaporation rate on the crystallization of poly (vinylidene fluoride) thin films. *Bull. Mater. Sci.* **2015**, *38*, 1093−1098.
(37) Sheng, H.; Liu, L.; Xu, J. Effect of graphene-doping and vacuum-annealing on the structure and properties of In: ZnO thin films. *Thin Solid Films* **2021**, *731*, 138760.
(38) Salam, M. A. E.; Elkomy, G. M.; Osman, H.; Nagy, M. R.; El-Sayed, F. Structure−electrical conductivity of polyvinylidene fluoride/graphite composites. *J. Reinf. Plast. Compos.* **2012**, *31*, 1342−1352.
(39) Ahmad, K.; Pan, W.; Shi, S. L. Electrical conductivity and dielectric properties of multiwalled carbon nanotube and alumina composites. *Applied physics letters* **2006**, *89*, 133122.
(40) Rozana, M. D.; Arshad, A. N.; Wahid, M. H.; Habibah, Z.; Ismail, L. N.; Sarip, M. N.; Rusop, M. Dielectric constant of PVDF/MgO nanocomposites thin films. In*IEEE Symposium on Business, Engineering and Industrial Applications*. 2012, pp 18-22.
(41) Zhang, H. B.; Zheng, W. G.; Yan, Q.; Yang, Y.; Wang, J. W.; Lu, Z. H.; Ji, G. Y.; Yu, Z. Z. Electrically conductive polyethylene terephthalate/graphene nanocomposites prepared by melt compounding. *Polymer* **2010**, *51*, 1191−1196.
(42) Green, R. *Hall effect measurements in materials characterization*, 2011, p 3111.

https://doi.org/10.1021/acsomega.3c00283
ACS Omega 2023, 8, 13876−13883

(43) Zhao, R.; Jayasingha, R.; Sherehiy, A.; Dharmasena, R.; Akhtar, M.; Jasinski, J. B.; Wu, S. Y.; Henner, V.; Sumanasekera, G. U. In Situ Transport Measurements and Band Gap Formation of Fluorinated Graphene. *J. Phys. Chem. C* **2015**, *119*, 20150−20155.
(44) Li, H.; Han, X.; Childress, A. S.; Rao, A. M.; Koley, G. Investigation of carrier density and mobility variations in graphene caused by surface adsorbates. *Physica E: Low-dimensional Systems and Nanostructures* **2019**, *107*, 96−100.
(45) Chen, J. H.; Jang, C.; Xiao, S.; Ishigami, M.; Fuhrer, M. S. Intrinsic and extrinsic performance limits of graphene devices on SiO_2. *Nature Nanotech* **2008**, *3*, 206−209.

https://doi.org/10.1021/acsomega.3c00283
ACS Omega 2023, 8, 13876−13883